Synthesis, Crystal Structure, and Characterization of $Ba(Ti_{1/2}Mn_{1/2})O_3$: A High Permittivity 12R-Type Hexagonal Perovskite

Gillian M. Keith,[†] Caroline A. Kirk,[‡] Kumaravinothan Sarma,[§] Neil McN. Alford,[§] Edmund J. Cussen,[||] Matthew J. Rosseinsky,[||] and Derek C. Sinclair*,[†]

Department of Engineering Materials, Sir Robert Hadfield Building, University of Sheffield, Mappin Street, Sheffield, United Kingdom, S1 3JD, Department of Mineralogy, The Natural History Museum, Cromwell Road, London, United Kingdom, SW7 5BD, Physical Electronics and Materials, London Southbank University, 103 Borough Road, London, United Kingdom, SE1 0AA, and Department of Chemistry, University of Liverpool, Liverpool, United Kingdom, L69 7ZD

Received December 12, 2003. Revised Manuscript Received February 26, 2004

A 12R-type hexagonal perovskite, $Ba(Ti_{1/2}Mn_{1/2})O_3$, has been prepared by a mixed oxide route at 1250 °C in air and the crystal structure established by a joint Rietveld refinement of powder X-ray and neutron diffraction data at room temperature [space group $R\bar{3}m$, $a =$ 5.69135(2) Å, and $c = 27.91860(15)$ Å]. The structure consists of a $(hhcc)_3$ stacking sequence of BaO_3 close-packed layers along the *c*-axis with face sharing M_3O_{12} trimers connected by a vertex sharing octahedron. Partial ordering of the Ti^{+IV} and Mn^{+IV} ions occurs in the B-site substructure; Mn^{+IV} ions occupy the central octahedral site in the trimers, Ti^{+IV} ions occupy the octahedral site in the vertex sharing octahedron, and both ions occupy the outer octahedral site of the trimers. Impedance spectroscopy and microwave dielectric resonance measurements on dense pellets (>97% of the theoretical X-ray density) show the title compound to be a modest dielectric insulator at room temperature with high permittivity, $\epsilon_r \sim 45$ (at both radio and microwave frequencies); a modest unloaded quality factor, $Q_u \sim$ 2026 (at ~5.75 GHz); and a temperature coefficient of resonant frequency, $TC_f = -4$ ppm K^{-1}.

Introduction

Oxides based on the perovskite structure are known to exhibit a diverse variety of useful properties such as ferro-, pyro-, and piezo-electricity; ionic and mixed ionic/electronic conductivity; superconductivity; and giant magnetoresistivity.[1] The ideal formula unit is ABO_3, where A is a large cation, e.g. K, Sr, Ba, La, and B is a smaller cation, e.g. Ti, Mn, Co, Ni, Cu, Ga, Zr, Nb, Ta. In general, many perovskites can be described in terms of a close-packed arrangement of AO_3 layers with B cations occupying octahedral sites. The stacking sequence of the AO_3 layers can be cubic (ABC), hexagonal (ABAB), or a combination of both. Perovskites based only on cubic close packing (ccp) of AO_3 layers leads to the familiar perovskite structure in which all BO_6 octahedra share corners, for example, $SrTiO_3$. This ccp structure is sometimes referred to as a 3C-polytype, as the repeat sequence of the ccp layers of octahedra in the unit cell is ccc, where c refers to corner-sharing octahedra. Those based only on hexagonal close packing (hcp) of AO_3 layers leads to infinite strings of face-sharing BO_6 octahedra parallel to the *c*-axis, for example $BaNiO_3$. This results in a two-layer hexagonal cell commonly denoted as 2H (or as hh in terms of packing of octahedra, where h refers to face-sharing octahedra). In general, 2H-type (hexagonal) perovskites are less common than 3C-type (cubic) perovskites, because of unfavorable electrostatic cation repulsion associated with the much shorter B−B distance between adjacent face-sharing octahedra in 2H-type compounds compared to that of vertex-sharing octahedra in 3C-type compounds.

Numerous combinations of mixed cubic (c) and hexagonal (h) stacking sequences are possible, resulting in a wide variety of perovskite-based structures containing both corner- and face-sharing BO_6 octahedra.[2−4] The unit cell of these layered structures is determined by the number (*n*) of AO_3 layers per cell. The symbols *n*L, *n*H, and *n*R are used to represent the number of layers and the symmetry, where L or H = hexagonal and R = rhombohedral. Many factors are known to influence the structure of perovskite-based materials, including hydrostatic pressure, the relative sizes of the A and B cations (r_A/r_B), their oxidation states and electronega-

* To whom correspondence should be addressed.
[†] University of Sheffield.
[‡] The Natural History Museum.
[§] London Southbank University.
[||] University of Liverpool.

(1) Moulson, A. J.; Herbert, J. M. *Electroceramics: Materials, Properties and Applications*; Chapman and Hall: London, 1990.
(2) Katz, L.; Ward, R. *Inorg. Chem.* **1964**, *3*, 205.
(3) Darriet, J.; Sbramanian, M. A. *J. Mater. Chem.* **1995**, *5*, 543.
(4) Donohue, P. C.; Katz, L.; Ward, R. *Inorg. Chem.* **1965**, *4*, 306.

10.1021/cm035317n CCC: $27.50
Published on Web 04/03/2004

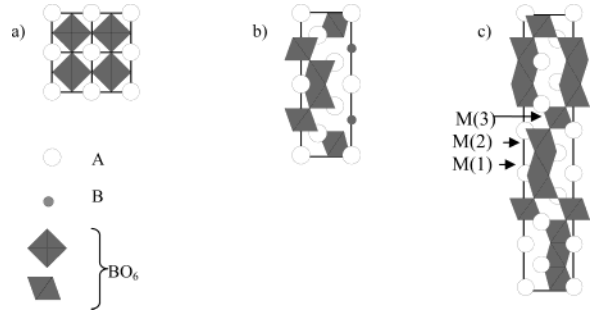

Figure 1. Structure of (a) 3C viewed along the [001] direction and (b) 6H and (c) 12R polytypes viewed along the [110] direction.

tivity, and the cation and anion content.[2,5−8] In general, an increase in corner-sharing octahedra and therefore %ccp occurs with increasing hydrostatic pressure or decreasing r_A/r_B and has been attributed to increased repulsion between cations in the face-sharing octahedra as the average size of the AO_3 layers decrease. This results in destabilization of face sharing octahedra and hence reduces the %hcp packing in mixed hcp and ccp perovskites.[5,6]

$BaTiO_3$ and $BaMnO_3$ are well-known perovskite-based materials that have been studied extensively. $BaTiO_3$ prepared at temperatures below ∼1430 °C is a tetragonally distorted 3C-type structure at room temperature, where the Ti ions are displaced from their centrosymmetric position within the corner-sharing TiO_6 network.[9] This gives rise to a dipole moment within the unit cell and via cooperative interactions leads to the development of ferroelectric domains. Tetragonal $BaTiO_3$ is a well-known ferroelectric material with a high relative permittivity at room temperature, ϵ'_r, (∼1000−3000), that finds numerous applications as a dielectric material in ceramic capacitors.[1] Above 130 °C it becomes cubic and paraelectric, and at ∼1432 °C it transforms to a 6H-type perovskite (space group $P6_3/mmc$) based on pseudo-close-packed BaO_3 layers, with a $(cch)_2$ stacking sequence that results in face-sharing Ti_2O_9 dimers connected by isolated TiO_6 corner-sharing units (Figure 1a). Undoped 6H-$BaTiO_3$ can be stabilized at room temperature, either by rapid quenching from >1500 °C[9] or by processing in low oxygen partial pressures at high temperatures (e.g 1300 °C, 0.1 mbar) to obtain oxygen-deficient materials, $BaTi^{+IV}{}_{1-x}Ti^{+III}{}_xO_{3-x/2}$ ($0 \le x \le 0.30$).[10] Alternatively, doped 6H-$BaTiO_3$-based materials can be obtained by partial replacement of Ti by a variety of cations including Mg, Mn, Fe, Co, Ni, and Ga.[11]

Stoichiometric $BaMnO_3$ can be prepared at ∼1000 °C and has the 2H structure; however, a sequence of $BaMnO_{3-x}$ (where $0 \le x \le 0.5$) layered compounds (2H → 15R → 8L → 6L → 10L → 4L) associated with oxygen loss at high temperatures was identified by X-ray diffraction.[12] From this study, it was suggested that structures with long face-sharing sequences, such as the 2H, 15R, and 8L compounds which contain infinite, five, and four strings of face-sharing octahedra, respectively, cannot tolerate large Mn^{3+} concentrations and oxygen vacancies within such long strings. Phase transformations therefore occur to increase the amount of corner sharing and thus produce structures with shorter face-sharing sequences, with Mn^{3+} ions and oxygen vacancies located in corner-sharing units to create square pyramidal coordination for the Mn^{3+} ions.

More recently, Parras et al.[13,14] used a combination of selected area electron diffraction (SAED) and high-resolution electron microscopy (HREM) to show a more complex picture for $BaMnO_{3-\delta}$ where oxygen deficiency could be accommodated either by disordered intergrowths of h-BaO_3 and c-$BaO_{2.5}$ layers or by formation of ordered hexagonal perovskite-related phases from intergrowths of MnO_6 octahedral and MnO_5 square pyramidal layers. In the latter case, the oxygen deficiency (x) is related to the number of layers by the equation $x = 0.5c(c + h)$ where $x < 0.22$ and c and h are the number of cubic and hexagonal layers, respectively. This model assumes that both the hexagonal and cubic layers always have fixed composition, BaO_3 and $BaO_{2.5}$, respectively, and that x determines the number of c-$BaO_{2.5}$ layers. Each structure-type in this model, therefore, has fixed oxygen content.

Perovskites containing mixed cubic/hexagonal stacking sequences have started to attract attention as dielectric resonators at microwave frequencies due to their high permittivity ($\epsilon' > 30$), low/moderate dielectric losses, or high Q (where $Q = 1/\tan\delta > 1000$ between 5 and 10 GHz), and near-zero temperature coefficient of resonant frequency ($|\tau_f| < 100$ ppm/K). For example, $Ba_5Nb_4O_{15}$ is a 5H-type structure with $\epsilon' = 39$, $Q = 5000$ (at 4.73 GHz), and $\tau_f = 78$ ppm K^{-1}.[15] Recently, 6H-$Ba(Ti_{0.92}Ga_{0.08})O_{2.96}$ ceramics have been reported to have encouraging microwave dielectric characteristics, with high room-temperature permittivity ($\epsilon'_r \sim 74$) and moderate losses ($Q \sim 1420$ at 5.5 GHz); however, its τ_f is rather high (550 ppm K^{-1}) due to the presence of subambient phase transitions.[16]

Recently, we have been investigating the $BaTiO_3$−$BaMnO_3$ system and have identified a new compound of composition $Ba(Ti_{1/2}Mn_{1/2})O_3$ which is a perovskite that crystallizes as a 12R polytype (space group $R\bar{3}m$) and consists of a $(hhcc)_3$ stacking sequence of BaO_3 close-packed layers that contains strings of three face-sharing octahedra connected by a corner-sharing octahedron (Figure 1b). To our knowledge there are relatively few reports of 12R-type oxides. Many of those that have been reported have been prepared under high oxygen partial pressure, such as $BaCrO_3$[17] and

(5) Longo, J. M.; Kafalas, J. A. *Mater. Res. Bull.* **1968**, *3*, 687.
(6) Longo, J. M.; Kafalas, J. A. *J. Solid State Chem.* **1969**, *1*, 103.
(7) Blasse, G. *J. Inorg. Nucl. Chem.* **1964**, *26*, 1191.
(8) Mitchell, R. H. *Perovskites: Modern and Ancient*; Almaz Press Inc: Onthario, Canada, 2002.
(9) Kirby, K. W.; Wechsler, B. A. *J. Am. Ceram. Soc.* **1991**, *74*, 1841.
(10) Sinclair, D. C.; Skakle, J. M. S.; Morrison, F. D.; Smith, R. I.; Beales, T. P. *J. Mater. Chem.* **1999**, *9*, 1327.
(11) Dickson, J. G.; Katz, L.; Ward, R. *J. Am. Chem. Soc.* **1961**, *83*, 3026.
(12) Negas, T.; Roth, R. S. *J. Solid Stat. Chem.* **1971**, *3*, 323.
(13) Gonzalez-Calbet, J. M.; Parras, M.; Alonso, J. M.; Vallet-Regi, M. *J. Solid State Chem.* **1994**, *111*, 202.
(14) Gonzalez-Calbet, J. M.; Parras, M.; Alonso, J. M.; Vallet-Regi, M. *J. Solid State Chem.* **1995**, *117*, 21.
(15) Kamba, S.; Petzelt, J.; Buixaderas, E.; Haubrich, D.; Vanek, P.; Kuzel, P.; Jawahar, I. N.; Sebastin, M. T.; Mohanan, P. *J. Appl. Phys.* **2001**, *89*, 3900.
(16) Feteira, A.; Sarma, K.; Alford, N. McN.; Reaney, I. M.; Sinclair, D. C. *J. Am. Ceram. Soc.* **2003**, *86*, 511.
(17) Chamberland, B. L. *Inorg. Chem.* **1969**, *8*, 286.

$BaFeO_{2.93}$,[18] or contain rather exotic and expensive metals, for example, Ir and Re in $Ba(Co_{1/2}Ir_{1/2})O_3$ and $A_4Re_2MO_{12}$, where A = Ba, Sr and M = Mg, Co and Zn, respectively.[19,20] Recently, a new hexagonal 12-layer Perovskite-related structure, $Ba_6R_2Ti_4O_{17}$ (where R = Nd and Y), has been reported[21] that contains pseudocubic (c′) BaO_2 layers in the sequence $(c'cchcc)_2$. The structure contains face-sharing Ti_2O_9 dimers connected by single RO_6 corner-sharing units that are connected by TiO_4 units that form around the c′-BaO_2 layers. Here we report details of the synthesis, thermal stability, crystal structure, and magnetic and electrical properties of 12R-$Ba(Ti_{1/2}Mn_{1/2})O_3$.

Experimental Section

Approximately 5-g batches of $Ba(Ti_{1-x}Mn_x)O_{3-\delta}$ for a range of x values were prepared by the mixed oxide route. For each composition, stoichiometric amounts of $BaCO_3$, TiO_2,and MnO_2 were weighed and mixed in an agate mortar and pestle with acetone. Samples were placed in platinum foil boats and decarbonated in a muffle furnace at 1000 °C for 2 h before being heated at 1250 °C for 14−16 h. The samples were then removed from the furnace at 1250 °C. This firing procedure at 1250 °C in air was repeated a total of three times with two intermittent grindings stages of 15 min. A 50-g ball-milled batch of $Ba(Ti_{1/2}Mn_{1/2})O_{3-\delta}$ ($x = 0.50$) powder was also prepared. Reagents were milled using yttria-stabilized zirconia milling media in a polypropylene pot with acetone. The reaction temperature and times were the same as for hand-ground samples. The ball-milled batch of powder was milled for a total of 10 h: an initial mill of 4 h to mix the reagents, followed by subsequent 2 h mills between and after firing.

X-ray analysis for phase identification was carried out using a Stoe STADI P diffractometer in transmission mode, Ge monochromator, Cu Kα1 radiation ($\lambda = 1.5408$ Å), and an Image Plate (IP) detector. Detailed X-ray diffraction (XRD) data for Rietveld refinement were also collected on the Stoe Stadi P diffractometer but using a small position sensitive diffractometer (PSD). Data were collected over the 2θ range 5−120°, with a step width of 0.01° and count-time of 45 s per step.

Neutron diffraction (ND) data for $Ba(Ti_{1/2}Mn_{1/2})O_{3-\delta}$ were collected on the diffractometer POLARIS at the ISIS facility (Rutherford Appleton Laboratories), from the highest resolution backscattering detectors, over the time-of-flight range 2000−19500 μs using cylindrical vanadium containers. The neutron scattering lengths for Ba, Ti, Mn, and O were taken from Sears.[22] Rietveld refinement[23] was carried out on both XRD and ND data for $Ba(Ti_{1/2}Mn_{1/2})O_{3-\delta}$ using the General Structural Analysis System (GSAS) suite of software.[24] The background levels of the diffraction patterns were fitted using a linear interpolation function for X-rays and a cosine Fourier series function for neutrons, and the peak shapes were described using a pseudo-Voigt function.

Hydrogen-reduction thermogravimetry was used to determine the oxygen content of $Ba(Ti_{1/2}Mn_{1/2})O_{3-\delta}$. A small sample of powder (60−70 mg) was placed in a Pt crucible within a Stanton Redcroft thermobalance (STA1500) and heated at 10 °C min^{-1} in a flowing 5% H_2/95% N_2 atmosphere (flow rate = 50−60 mL min^{-1}) from room temperature to 1000 °C. The sample was held at 1000 °C for 10 min to achieve constant weight before cooling back to room temperature in the same atmosphere at a cooling rate of 10 °Cmin^{-1}.

Magnetic measurements on $Ba(Ti_{1/2}Mn_{1/2})O_{3-\delta}$ were carried out using a Quantum Design MPMS XL-7T SQUID operating at a field of 200 Oe. Zero-field-cooled (ZFC) and field-cooled (FC) data were collected on heating from 4 to 300 K.

Pellets of $Ba(Ti_{1/2}Mn_{1/2})O_{3-\delta}$ were prepared by pressing ball-milled powder in a uniaxial die under a load of 0.2 tons for approximately 3 min followed by sintering at 1450 °C for 2 h in flowing oxygen using a heating and cooling rate of 5 °C min^{-1}. Pellet density was estimated from the mass and dimensions of the sintered bodies and the ceramic microstructure was characterized using an optical microscope. Pellets were polished and then etched using an etchant of 0.5 mL of HF plus 9.5 mL of HNO_3 in 150 mL of distilled water prior to mounting under the microscope.

The electrical properties were measured from a combination of fixed frequency (10 kHz) capacitance measurements at 1 V from 300 to 800 K using an LCR meter (HP model 4284A), impedance spectroscopy (IS) over a frequency range from 5 Hz to 13 MHz at 0.1 V from 80 to 1000 K using an HP LF 4912A impedance analyzer, and microwave dielectric measurements at 300 K by the resonant cavity method using a network analyzer (HP Model 8720 D). Prior to LCR and IS measurements, the major pellet faces were coated with an organo-Pt paste and were fired at 1000 °C for 1 h to burn-out the organic residues to form hardened Pt-metal electrodes. The samples were mounted on in-house conductivity rigs and placed either inside an noninductively wound furnace (for measurements >300 K) or in an Oxford Instruments Optistat bath cryostat (for measurements <300 K). Temperature control was ±2 °C in both setups.

Results

XRD revealed an interesting sequence of mixed cubic/hexagonal perovskites for samples of $Ba(Ti_{1-x}Mn_x)O_{3-\delta}$ prepared at 1250 °C in air. For $x < 0.04$, single-phase 3C-$BaTiO_3$ was observed, followed by single-phase 6H between $x = 0.05$ and $x = 0.10$. A narrow two-phase region exists between the 3C and 6H solid solutions. The next single-phase composition occurred at $x = 0.50$, where the XRD pattern fully indexed on a 12R cell with lattice parameters $a = 5.69$ Å, $c = 27.92$ Å, and space group $R\bar{3}m$. Convergent beam electron diffraction demonstrated the 3-fold symmetry expected from this space group (not shown), confirming a 12R-type as opposed to 12L-type structure. All compositions in the range $0.10 < x < 0.50$ were phase mixtures of 6H and 12R. The Mn-rich part ($x > 0.50$) of the phase diagram is still under investigation, but $x = 0.75$ is a phase mixture of 12R and 9R polytypes. The end member ($x = 1$) is a mixture of 15R and 21R, which is in good agreement with that reported by Parras et al.[13] for $BaMnO_{3-\delta}$ prepared at 1250 °C in air. Full details of the complete phase diagram will be discussed elsewhere.[25] Here we report results for the 12R phase identified at $x = 0.50$.

At temperatures above 1250 °C, the phase assemblage for $x = 0.50$ is atmosphere dependent. Samples heated in air at 1400 °C are a mixture of 12R and 6H, whereas single-phase 12R is maintained for samples heated in flowing O_2 at 1450 °C. Postannealing phase mixtures in air at 1250 °C for >3 days after heating at 1400 °C in air does not lead to complete reformation of single-phase 12R; some 6H is always present.

Hydrogen reduction TGA was carried out to establish the oxygen content of $Ba(Ti_{1/2}Mn_{1/2})O_{3-\delta}$ prepared at 1250 °C in air. A total mass loss of ~3.3% was recorded for a sample reduced to a constant weight at 1100 °C.

(18) Takeda, Y.; Shimada, M.; Kanamaru, F.; Koizumi, M. *J. Solid State Chem.* **1973**, *7*, 229.
(19) Vente, J. P.; Battle, P. D. *J. Solid State. Chem.* **2000**, *152*, 361.
(20) Longo, J. M.; Katz, L.; Ward, R. *Inorg. Chem.* **1965**, *4*, 235.
(21) Kuang, X.; Jing, X.; Loong, C.-K.; Lachowski, E. E.; Skakle, J. M. S.; West, A. R. *Chem. Mater.* **2002**, *14*, 4359.
(22) Sears, V. F. *Neutron News* **1992**, *3*, 26.
(23) Rietveld, H. M. *J. Appl. Crystallogr.* **1969**, *2*, 65.
(24) Larson, A. C.; von-Dreele, R. B. *General Structural Analysis System (GSAS), Report LAUR 86-748;* Los Alamos National Laboratories, 1990.

Table 1. Structural Parameters of $BaTi_{1/2}Mn_{1/2}O_3$ at Room Temperature[a]

atom	site	site occupancy	*x*	*y*	*z*	U_{iso} (Å^2)
Ba(1)	6c	1.0	0	0	0.285 382(32)	0.005 78(16)
Ba(2)	6c	1.0	0	0	0.129 045(31)	0.004 70(14)
M(1)	3b	0.5/0.5	0	0	1/2	0.001 76(17)
M(2)	6c	0.5/0.5	0	0	0.408 589(44)	0.004 30(16)
M(3)	3a	0.5/0.5	0	0	0	0.005 46(25)
O(1)	18h	1.0	0.149 089(33)	0.850 911(33)	0.456 580(17)	0.005 63(7)
O(2)	18h	1.0	0.167 438(55)	0.832 561(55)	0.626 589(17)	0.006 02(6)

[a] Space group $R\bar{3}m$; $a = b = 5.691\ 35(2)$ Å, $c = 27.918\ 60(15)$ Å, $V = 783.168(4)$ Å^3. Total agreement indices: $R_{wp} = 3.15\%$, $R_p = 4.04\%$. $\chi^2 = 1.625$ for 38 variables. The metal site occupancy cannot be distinguished from the site scattering powers, although as discussed in the text it is possible to infer the cation distribution from the metal−oxygen distances.

Table 2. Selected Bond Lengths (Å) and Angles (deg) for $BaTi_{1/2}Mn_{1/2}O_3$ Calculated from Rietveld Refinement of X-ray and Neutron Diffraction Data

M(1)−O(1) ×6	1.9051(4)	Ba(1)−O(1) ×6	2.85554(6)	M(1)−M(2)	2.5521(12)
M(2)−O(1) ×3	1.9888(10)	Ba(1)−O(1) ×3	2.9014(7)	M(2)−M(3)	3.9002(7)
M(2)−O(2) ×3	1.9206(8)	Ba(1)−O(2) ×3	2.9739(9)		
M(3)−O(2) ×6	1.9815(5)	Ba(2)−O(2) ×6	2.85417(8)	O(1)−O(1)	2.5456(6)
		Ba(2)−O(2) ×3	2.9605(9)	O(2)−O(2)	2.7717(9)
		Ba(2)−O(1) ×3	2.7781(8)		
O(1)−M(1)−O(1)	83.839(18)	O(1)−M(2)−O(1)	79.58(4)	O(2)−M(3)−O(2)	91.244(21)
M(1)−O(1)−M(1)	83.75(6)	O(2)−M(2)−O(2)	96.19(5)		
		O(1)−M(2)−O(2)	168.40(6)		

XRD showed the final products from the reduction process to be Ba_2TiO_4 and MnO. The composition for $x = 0.50$ was determined to be $Ba(Ti_{1/2}Mn_{1/2})O_{2.98(2)}$, indicating the compound to be oxygen stoichiometric within experimental errors.

A combined structural refinement of XRD and ND data was carried out, refining in the space group $R\bar{3}m$ and using the structural parameters of $BaIr_{0.5}Co_{0.5}O_{3-\delta}$ from Vente and Battle[19] as a starting model. Initially, the isotropic displacement parameters of each atom type (Ba, (Ti/Mn) and O) were constrained to be equal and the total occupancies of each site fixed to 1. The structural model has three unique B sites where the Mn and Ti atoms will be located. As the X-ray scattering factors and neutron scattering lengths (Ti = −3.438 fm, Mn = −3.73 fm) for these two atoms are very similar, making it difficult to distinguish between them using either diffraction technique, an equal distribution of Ti and Mn over the three B-sites was used in the starting model.

The atomic positions and displacement parameters were allowed to refine, and once a stable point had been reached, the constraints on the displacement parameters were removed and the refinement continued until a stable minimum was achieved. The O(1) and O(2) site occupancies were allowed to refine during the course of the refinement; however, within errors the refined values indicated that both oxygen sites were fully occupied, in good agreement with the TGA results, and were constrained to unity in the final refinement.

The refined atomic positions, occupancies, and displacement parameters for 12R-$Ba(Ti_{1/2}Mn_{1/2})O_3$ resulting from the Rietveld refinement of powder X-ray and neutron diffraction data are listed in Table 1 and selected, calculated bond lengths and angles are listed in Table 2. The displacement parameters for the three B-sites do show some spread in their values; however, allocation of higher proportions of Ti or Mn to a particular B-site did not improve the refinement. The observed, calculated, and difference profiles for both XRD and ND are shown in Figure 2. A good fit between

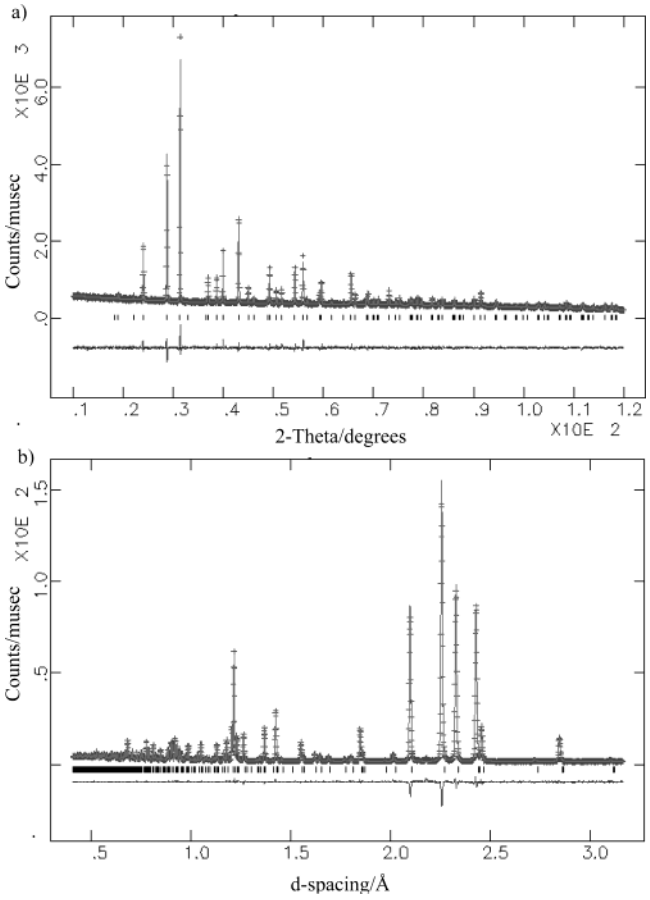

Figure 2. Observed, calculated, and difference (a) X-ray and (b) neutron diffraction patterns of 12R-$BaTi_{1/2}Mn_{1/2}O_3$ at room temperature. Reflection positions are marked.

calculated and experimental data was achieved, as highlighted by the low *R*-values, $R_p = 3.15\%$ and $R_{wp} = 4.04\%$, and the goodness-of-fit parameter, $\chi^2 = 1.625$.

Bond valence sum (BVS) calculations were performed using bond lengths from Table 2. As the material appeared to be fully oxygenated by both Rietveld refinement of ND data and by H_2-reduction TGA, VBS were performed only for Ti^{+IV} and Mn^{+IV} ions. The values

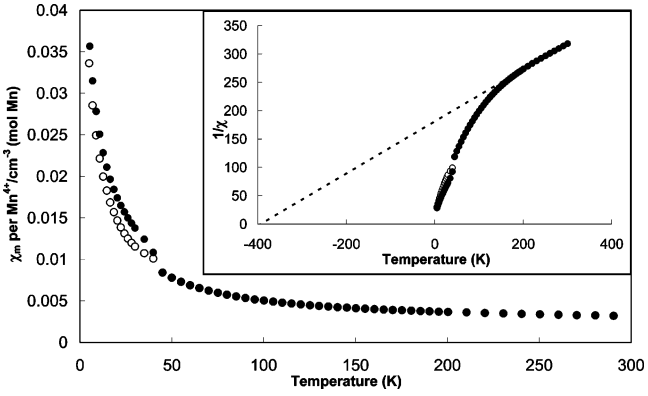

Figure 3. Temperature dependence of FC (filled symbols) and ZFC (open symbols) magnetic susceptibility of 12R-$BaTi_{1/2}Mn_{1/2}O_3$. The inset shows the fit to the high-temperature data using the Curie−Weiss law.

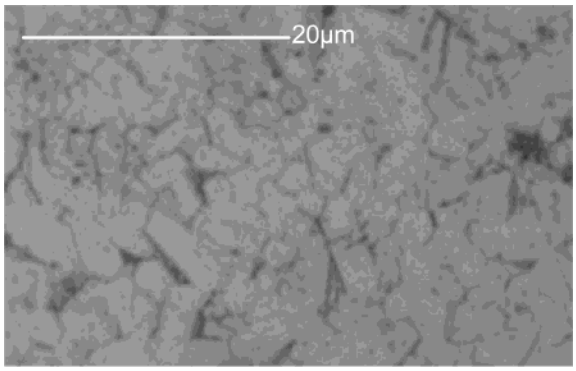

Figure 4. Optical micrograph of a chemically etched surface of a 12R-$BaTi_{1/2}Mn_{1/2}O_3$ ceramic.

Table 3. Bond Valence Sums for Ti and Mn in 12R-$BaTi_{1/2}Mn_{1/2}O_3$

	M(1) site $00^1/_2$	M(2) site 00*z*	M(3) site 000
$\sum V_{Mn-O}$	3.98	3.49	3.24
$\sum V_{Ti-O}$	4.70	4.13	3.83

listed in Table 3 indicate Mn ions to have a strong preference for the central site of the face-sharing trimers, M(1) site, whereas Ti ions have a stronger preference for the outer sites of the face-sharing trimers, M(2) site, and for the vertex-sharing octahedron, M(3) site.

The temperature dependence of the molar magnetic susceptibility was measured in 200 Oe between 4 and 300 K and is shown in Figure 3. The inset shows the inverse susceptibility as a function of temperature. The ZFC and FC data overlie above >150 K and obey the Curie−Weiss law over this temperature range (inset Figure 3). The Weiss temperature is strongly negative, indicating antiferromagnetic interactions and $\mu_{eff} = 4.17$ μ_B per Mn. The susceptibility at lower temperatures is more complex, being higher than that predicted from extrapolation from the higher temperature Curie−Weiss regime. No maximum is observed in the susceptibility; however, divergence of the FC and ZFC data occurs at ∼45 K.

Ceramics prepared for electrical measurements were >97% of the theoretical X-ray density, and optical microscopy of chemically etched surfaces revealed a ceramic microstructure consisting of uniform, regular shaped grains of 5−10 μm (Figure 4). The ceramics were too resistive (>10^7 Ω cm) to measure by impedance

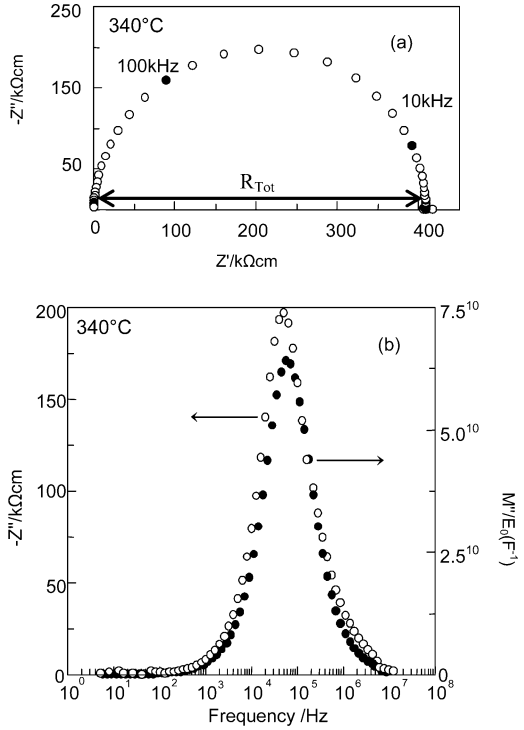

Figure 5. (a) Complex impedance plane plot and (b) a combined *Z*″, *M*″ spectroscopic plot for 12R-$BaTi_{1/2}Mn_{1/2}O_3$ ceramics at 340 °C. Selected frequencies (in Hz) are shown as filled symbols in part a.

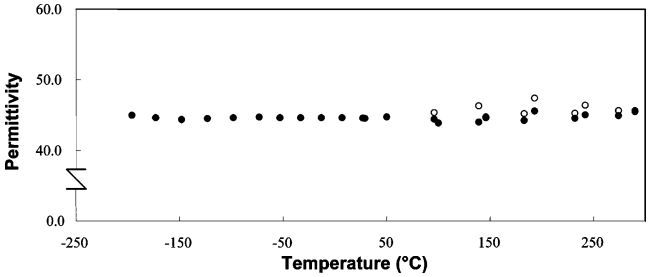

Figure 6. Relative permittivity as a function of temperature for 12R-$BaTi_{1/2}Mn_{1/2}O_3$. Filled symbols are from fixed frequency capacitance data (1 MHz) and open symbols are from high-frequency *M*′ intercepts of *M** plane plots from impedance spectroscopy data.

spectroscopy (IS) at room temperature. Complex plane (*Z**) plots of impedance data at elevated temperatures showed the presence of a single, semicircular arc that could be modeled on an equivalent circuit consisting of a single parallel RC element (Figure 5a). The arc had an associated capacitance of ∼3−4 pF cm^{-1} (from the relationship $\omega RC = 1$ at Z''_{max}, where $\omega = 2\pi f$ and *f* is the applied frequency), indicative of a bulk response with a permittivity of ∼40−50. The electrical homogeneity of the ceramics was confirmed by the presence of single, Debye-like peaks occurring at similar frequencies in spectroscopic plots of the imaginary components of the impedance, *Z*″, and electric modulus, *M*″ (Figure 5b). The bulk permittivity estimated from *M** plots at elevated temperatures and from fixed frequency (1 MHz) capacitance measurements at lower temperature was ∼45 and showed very little temperature dependence (Figure 6). The bulk resistivity at elevated temperatures was calculated from the intercept of the arc on the real axis, *Z*′, at low frequencies in *Z** plots. An Arrhenius plot of the bulk conductivity, σ, (where $\sigma =$

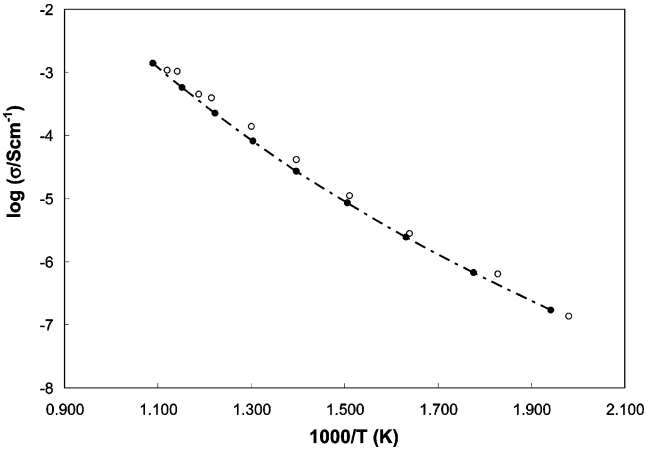

Figure 7. Arrhenius plot of bulk conductivity for 12R-$BaTi_{1/2}Mn_{1/2}O_3$. Heating and cooling data are shown by filled and open symbols, respectively.

$1/R$) shows slight curvature over the measured temperature range (Figure 7). An activation energy associated with the conduction process of 1.02(3) eV was estimated from the slope of the high-temperature data.

Microwave dielectric resonance measurements at room temperature showed the samples to resonate at ~5.75 GHz, with $\epsilon_r \sim 45$ and $Qf_u \sim 2026$ GHz. τ_f was measured over the temperature range 250−300 K and was established to be -4 ppm K^{-1}.

Discussion

The discovery of a 12R-type hexagonal perovskite ($x = 0.50$) was an interesting feature of the $Ba(Ti_{1-x}Mn_x)O_{3-\delta}$ system. 12R-polytypes appear to be relatively uncommon, given the few examples previously reported. Rietveld refinement was carried out on 12R-$BaTi_{0.50}Mn_{0.50}O_{3-\delta}$ using the structural parameters of $Ba(Ir_{0.50}Co_{0.50})O_{3-\delta}$ reported by Vente and Battle[19] as a starting model. The refinement progressed well and provided several details regarding the structure of this material.

Refinements of the oxygen content did not reveal any significant evidence for oxygen vacancies, which supports the results from thermogravimetric analysis; therefore, both oxygen sites were refined to be fully occupied and the compound is essentially oxygen stoichiometric for samples prepared at 1250 °C. Although not studied in detail, it would appear that 12R-$Ba(Ti_{1/2}Mn_{1/2})O_3$ cannot tolerate significant levels of oxygen loss, as decomposition into a phase mixture was observed from XRD for samples heated in air at >1300 °C.

Selected bond lengths and angles from the Rietveld refinements of powder XRD and ND are given in Table 2. In-plane Ba−O distances are very similar, with values of 2.85554(6) Å for h-$[Ba(1)-O(1)]_3$ and 2.85417(8) Å for c-$[Ba(2)-O(2)]_3$. The interplane Ba−O distances range from 2.7781(8) to 2.9739(3) Å, which are typical Ba−O bond lengths in close-packed BaO_3 layer-type structures.[10,19,26] It is interesting to note that the M(1) and M(3) sites corresponding to the central octahedron of the $(Ti,Mn)_3O_{12}$ trimers and the vertex-sharing octahedron (Figure 1c), respectively, have very different M−O bond lengths; the M(1)−O(1) bond length is 1.9051(4) Å compared to 1.9815(5) Å for M(3)−O(2). The M(2) sites in the terminal positions in the trimers have three M(2)−O(1) bond lengths of 1.9888(10) Å and three M(2)−O(2) bond lengths of 1.9206(8) Å (Table 2).

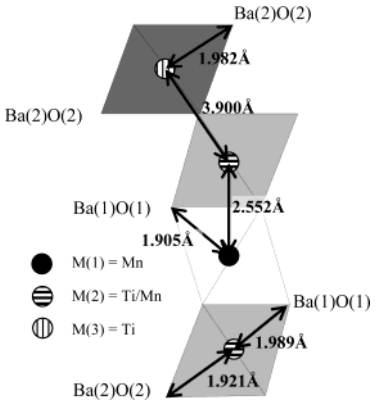

Figure 8. Schematic diagram illustrating the B-site cation arrangement and selected metal−oxygen and metal−metal distances in 12R-$BaTi_{1/2}Mn_{1/2}O_3$.

Octahedral site occupancies could not be refined due to the similarity in neutron and X-ray scattering lengths of Ti and Mn; therefore, BVS calculations were used to try and establish any site preference(s) for the Ti and Mn ions. These are shown in Table 3 and demonstrate that the Mn^{+IV} ions have a strong preference for the central position in the M_3O_{12} trimers and are unlikely to occupy the M(3) site, where they would be strongly underbonded, whereas the Ti^{+IV} ions show a preference for the M(2) and M(3) sites (Table 3). On the basis of this analysis, it seems reasonable to suggest a B-site distribution where the M(1) sites are occupied only by Mn^{+IV} ions, the M(3) sites are occupied only by Ti^{+IV} ions, and the M(2) sites are occupied by a mixture of Mn^{+IV} and Ti^{+IV} ions. Figure 8 summarizes this distribution and includes selected Ti/Mn−O bond lengths and metal−metal distances. The Mn−O bond length of 1.9051(4) Å for the central octahedron in the trimers, $M(1)-O(1)_6$, is in excellent agreement with that observed for Mn^{+IV} ions in the infinite chains of face−sharing octahedra parallel to the c axis in 2H-$BaMnO_3$ (1.9044(4))[26] and in the central octahedron of Mn_3O_{12} trimers in 9R-$BaMnO_3$ (1.906(4)).[27] The Ti−O bond length of 1.9815(5) for the single corner-sharing octahedron, $[M(3)-O(2)]_6$, is typical of that observed in cubic- and hexagonal-type titanate-based perovskites and is in excellent agreement with that observed for the vertex-sharing octahedron in undoped 6H-$BaTiO_3$ (1.983(5) Å),[10] (Figure 1b). The M−O bond distances associated with the M(2) site in the terminal positions of the trimers are also typical of those observed for Mn^{+IV} and Ti^{+IV} ions in oxides, for example, $Ba_6Mn_5O_{16}$.[28]

The short M−M distance of 2.5521(12) Å between adjacent face-sharing octahedra within the trimers is intermediate between that observed for adjacent face-sharing octahedra in the infinite chains of 2H-$BaMnO_3$ (2.4074(1) Å)[26] and for face-sharing dimers in 6H-$BaTiO_3$ (2.690(4) Å).[29] As the proposed cation distribu-

(25) Keith, G. M.; Sinclair, D. C. Unpublished results.
(26) Cussen, E.; Battle, P. D. *Chem. Mater.* **2000**, *12*, 831.
(27) Boullay, Ph.; Hervieu, M.; Labbe, Ph.; Raveau, B. *Mater. Res. Bull.* **1997**, *32*, 35.
(28) Boulahya, K.; Parras, M.; Gonzalez-Calbet, J. M.; Martinez, J. L. *Chem. Mater.* **2002**, *14*, 4006.

tion with 100% of the central site being Mn and 50% of the terminal site being Ti would give a population of 50% Mn−Ti and 50% Mn−Mn pairs in adjacent face-sharing sites, this is suggestive that the distribution proposed on the basis of valence sums is realistic. In 2H-$BaMnO_3$ (100% hcp), there is no possibility for cooperative displacement of the B-site cations from the center of their octahedral sites along the *c*-axis to relieve electrostatic repulsion within the infinite face-sharing strings, and consequently, the M−M distance is short (∼2.40 Å). In 12R-$Ba(Ti_{1/2}Mn_{1/2})O_3$, the occurrence of ccp creates vertex-sharing octahedra (Figure 8), which assists in reducing electrostatic repulsion between the B-site cations in adjacent face-sharing octahedra by facilitating the cations at the end of the M_3O_{12} trimers to displace away from the center of their octahedral sites and hence away from the shared face with the M(1) site in the center of the trimers, resulting in an increase in the M−M distance (Figure 8). In 6H-$BaTiO_3$, the electrostatic repulsion within the face-sharing units is further reduced because both cations within the dimers (Figure 1b) are displaced away from the center of their octahedral sites and hence away from the shared face, and the M−M distance increases to ∼2.69 Å. The shortest O−O distance (2.5456(6) Å) in 12R-$Ba(Ti_{1/2}Mn_{1/2})O_3$ occurs in the h-[Ba(1)−O(1)]$_3$ layers and is similar to that observed for 2H-$BaMnO_3$ (2.5561(9)Å)[26] and is a result of the oxide ions moving to partially screen the electrostatic repulsion between the Mn(1) and Mn/Ti(2) cations within the face-sharing trimers.

A magnetic moment per manganese ion in 12R-$Ba(Ti_{1/2}Mn_{1/2})O_3$ of 4.17 μ_B was calculated from the Curie−Weiss response (Figure 3, inset), over the given temperature range. On the basis of the spin-only formula, this value is slightly higher than the 3.89 μ_B expected for Mn^{4+} (d^3), and given the restricted range of applicability of the Curie−Weiss law, this is consistent with the results obtained from TGA and Rietveld refinements of XRD and ND data. The negative Θ value of −350 K indicates very strong antiferromagnetic interactions, and the sample is not therefore strictly in the Curie−Weiss limit over the measured temperature range. As only a second-order orbital contribution to the moment of Mn^{+IV} is expected, the Θ value is associated with antiferromagnetic (AF) interactions rather than complexities due to single ion magnetism. The presence of nonmagnetic Ti^{+IV} ions in the octahedral sites presumably prevents any possibility of cooperative long-range magnetic ordering of the Mn^{+IV} ions within the chains along the *c*-axis, and this is consistent with the absence of a maximum in the susceptibility attributable to long-range magnetic ordering. Below 150 K, the exchange between the manganese ions becomes sufficiently strong that the Curie−Weiss assumptions based on magnetic response by single weakly coupled ions break down, although the material remains paramagnetic down to ∼45 K. This can be ascribed to the formation of exchange-coupled pairs and trimers of manganese ions within the face-sharing blocks in the hexagonal parts of the structure. The increase in gradient of the inverse susceptibility below 150 K is compatible with total spin cancellation in manganese dimers and the magnetic monomers and trimers each exhibiting an uncompensated spin of $S = 3/2$. Such a description, however, neglects the possibilities of imperfect cancellation of spins within the dimers, extended interactions between trimers leading to magnetic cluster formation, and variability in local exchange interactions due to cation disorder within the material. Such a quantitative assignment must, therefore, be considered to be speculative.

The divergence between ZFC and FC data below ca. 45 K is most likely due to a small quantity of the ferrimagnetic spinel phase Mn_3O_4, $T_c = 43$ K,[30] which is undetectable by either the X-ray or neutron powder diffraction data or by optical microscopy. Such a small quantity would have a negligible effect on the stoichiometry of the 12R phase.

The main point of interest in the magnetic susceptibility is the apparent absence of a transition from a dynamic Curie−Weiss type paramagnetic regime (observed for $T > 150$ K) to a static spin structure of either an antiferromagnetically ordered phase or a spin glass. This appears to contradict the strong magnetic interactions indicated by the large magnitude of the Weiss constant. This Weiss constant is in good agreement with the superexchange observed in the 4H phase $SrMnO_3$,[31] which showed antiferromagnetic coupling between Mn^{+IV} cations across a shared octahedral face at ca. 350 K while the coupling across a shared corner occurred at $T = 278(5)$ K, leading to the formation of an antiferromagnetic phase. This strong coupling between Mn^{+IV} cations across a shared octahedral face is likely to persist in the 12R phase $BaTi_{0.5}Mn_{0.5}O_3$, but the long-range magnetic properties will be modified by the presence of diamagnetic Ti^{4+} on some of the octahedral sites.

The effect of cation disorder in mixed cubic/hexagonal perovskites was studied in the 15R phase $SrMn_{0.9}Fe_{0.1}O_{3-\delta}$.[32] This material showed antiferromagnetic order between the Mn cations, which predominantly occupy the face-sharing octahedral sites, but the Fe cations, which favored the corner-linked octahedra, remained paramagnetic down to 5 K, despite being embedded in a magnetically ordered matrix. This shows considerable similarities with the 12R phase under discussion. The chemical disorder indicated by the large variation in M−O distances results in a number of different magnetic environments for Mn^{4+} with zero, one, or two Mn^{+IV} cations in adjacent face-sharing sites. This randomization of exchange interactions could lead to a weak net interaction and allows the magnetic moments on Mn^{+IV} to remain dynamically disordered over the full temperature range studied.

The microstructure of $Ba(Ti_{1/2}Mn_{1/2})O_3$ (Figure 4) exhibits some anisotropic grain growth, with grains of ∼5 × 10 μm, but no exaggerated anisotropic grain growth was observed. This is in contrast to 6H-$Ba(Ti_{0.95}Mn_{0.05})O_3$, in which extensive anisotropic grain growth has been observed.[33] In the case of 12R-$Ba(Ti_{1/2}Mn_{1/2})O_3$, ceramics were processed in a flowing oxygen gas

(29) Akimoto, J.; Gotoh, Y.; Oosawa, Y. *Acta Crystallogr. Sect. C* **1994**, *50*, 160.

(30) Goodenough, J. B. *Magnetism and the Chemical Bond*; Wiley: New York, 1963.

(31) Chamberland, B. L.; Sleight, A. W.; Weiher, J. F. *J. Solid State Chem.* **1970**, *1*, 506.

(32) Cussen, E. J.; Sloan, J.; Vente, J. P.; Battle, P. D.; Gibb, T. C. *Inorg. Chem.* **1998**, *37*, 6071.

atmosphere in an attempt to limit oxygen loss and therefore to suppress anisotropic grain growth occurring by an oxygen-loss mechanism, as has been recently suggested for several 6H- and 3C-$BaTiO_3$-based materials.[34]

The room-temperature permittivity of 12R-$Ba(Ti_{1/2}Mn_{1/2})O_3$ is moderately high, $\epsilon_r' \sim 45$, and shows very little temperature dependence over a ~500 °C temperature range from −200 to 300 °C (Figure 6). Impedance spectroscopy was used to characterize the bulk electrical properties at elevated temperatures and revealed 12R-$Ba(Ti_{1/2}Mn_{1/2})O_3$ to be a modest dielectric. An Arrhenius plot of the bulk conductivity (Figure 7) showed slight curvature at lower temperatures, indicating that the conduction mechanism is not a simple band-gap model, at least at low temperatures. Variable range hopping models for both two- and three-dimensional conduction[35] were applied to the data; however, these also showed deviations from linearity. The nonlinearity of the conductivity plots implies that the electrical response does not fully fit any of the applied models. The change in slope may be associated with a change in conduction mechanism over the temperature range studied. The linear Arrhenius-type response at high temperature may be intrinsic conduction associated with ionization of carriers from the valence band to the conduction band with a band gap of ~2 eV ($E_g \sim 2E_a$), whereas at lower temperatures an extrinsic conduction mechanism may arise due to the presence of impurities or perhaps a small concentration of Mn^{+III} ions resulting in polaron hopping between Mn^{+III} and Mn^{+IV} ions.

Dielectric resonance was obtained at GHz frequencies and ceramics had $\epsilon' \sim 45$, $Q \sim 2026$ (at 5.75 GHz), and $TC_f \sim -4$ ppm K^{-1}. Although microwave dielectric resonance has been reported for a variety of hexagonal-type perovskites, e.g. 5L, 6L, 8L, and 18L compounds, as far as we are aware, this is the first report of microwave dielectric resonance in a 12-layer hexagonal perovskite-type material. The microwave dielectric properties of 12R-$Ba(Ti_{1/2}Mn_{1/2})O_3$ are quite similar to 5-layer $La_4BaTi_4O_{15}$,[36] which has $\epsilon_r \sim 43$, $Q \sim 1430$ (at 8.1 GHz), and $TC_f \sim -17$ ppm K^{-1}, and 18-layer $La_4Ba_2Ti_5O_{18}$,[36] with $\epsilon_r \sim 46$, $Q \sim 4010$ (at 7.94 GHz), and $TC_f \sim -36$ ppm K^{-1}. Although other hexagonal-type perovskites can have significantly higher room-temperature permittivity values, e.g. 6H-$Ba(Ti_{0.95}Mn_{0.05})O_3$ has $\epsilon_r \sim 70$ with $Q \sim 1600$ (at 4.8 GHz),[33] many of these undergo structural phase transitions that result in very high TC_f values, e.g. ~500 ppm K^{-1} for 6H-$Ba(Ti_{0.92}Ga_{0.08})O_{2.96}$,[16] and this precludes them from most commercial applications that require near-zero values of TC_f.

Many factors can influence the dielectric resonance properties of ceramics. At present, several factors that influence ϵ', Q, and TC_f for 3C-type perovskites are reasonably well established. For example, highly polarizable d^0 cations such as Ti, Nb, and Ta on the B-site are known to favor high ϵ', strict cation ordering on the B-site substructure of complex B-site perovskites is known to optimize Q, and control of the octahedral tilt system using tolerance factor considerations (i.e. r_A/r_B) can be used to tailor $TC_f \sim 0$ ppm K^{-1}. On this basis, the high permittivity of 12R-$Ba(Ti_{1/2}Mn_{1/2})O_3$ can be rationalized to the presence of Ti^{+IV} ions on the B-site of the structure, and the modest Q value can be related to the fact that this material is a poor dc insulator at room temperature and that there is incomplete ordering of the Ti^{+IV} and Mn^{+IV} ions on the B-site substructure (Figure 8). At this stage, however, the reason(s) why TC_f is close to zero is not obvious but is presumably related to the absence of any structural phase transition near room temperature and to restricted tilting in the octahedral network. The low Q of this material will preclude any commercial applications of 12R-$BaTi_{1/2}Mn_{1/2}O_3$ as a microwave dielectric resonator; however, this study is a further demonstration that hexagonal-type perovskites can produce high permittivity materials with near-zero TC_f values.

It is noteworthy that high Q values of ~20 800 (at 3.3 GHz) have recently been reported for an 8-layer hexagonal-type perovskite, $Ba_8Ta_6ZnO_{24}$.[37] In this case, the Ta and Zn ions are ordered on the B-site substructure, and this demonstrates a clear link between Q and B-site cation ordering in hexagonal-type perovskites. In general, the structure−composition−dielectric property relationships of hexagonal-type perovskites have received very little attention; however, the prospect remains that such materials (especially those containing highly polarizable B-site cations in an ordered arrangement) may have similar and possibly superior microwave dielectric resonance properties to 3C-type perovskites such as $Ba(Zn_{1/3}Ta_{2/3})O_3$[38] (where $\epsilon' \sim 30$, $TC_f \sim 0$ ppm K^{-1}, and $Q > 50\,000$ (at 2 GHz) and therefore lead to a new generation of high-permittivity, low-loss microwave dielectric resonators.

Conclusions

A 12R-type hexagonal perovskite with composition $Ba(Ti_{1/2}Mn_{1/2})O_{3-\delta}$ has been prepared by a mixed oxide route at 1250 °C in air. Hydrogen reduction thermogravimetry, Rietveld refinement of ND data, and magnetic susceptibility measurements all suggest the compound to be essentially oxygen stoichiometric, within experimental errors. Rietveld refinement of powder XRD and ND data (space group $R\bar{3}m$, $a = 5.69135(2)$ Å, and $c = 27.91860(15)$ Å) showed the structure to consist of a $(hhcc)_3$ stacking sequence of BaO_3 close-packed layers along the c-axis with face-sharing M_3O_{12} trimers connected by a vertex-sharing octahedron. Partial ordering of the Ti^{+IV} and Mn^{+IV} ions occurs on the B-site substructure, with the smaller Mn^{+IV} ions occupying the central octahedral site in the trimers, the larger Ti^{+IV} ions occupying the octahedral site in the vertex sharing octahedron,and both ions occupying the outer octahedral site of the trimers.

Magnetic susceptibility measurements from 4 to 300 K do not show any evidence for cooperative long-range

(33) Keith, G. M.; Rampling, M. J.; Sarma, K.; Alford, N. McN.; Sinclair, D. C. *J. Eur. Ceram. Soc.* In press.
(34) Langhammer, H. T.; Müller, T.; Felgner, K.-H.; Abicht, H.-P. *J. Am. Ceram. Soc.* **2000**, *83*, 605.
(35) Mott, N. F.; Davis, E. A., *Electronic Processes in Non-Crystalline Materials;* Oxford University Press: London, 1979.
(36) Vineis, C.; Davies, P. K.; Negas, T.; Bell, S. *Mater. Res. Bull.* **1996**, *31*, 431.
(37) Moussa, S. M.; Claridge, J. B.; Rosseinsky, M. J.; Clarke, S.; Ibberson, R. M.; Price, T.; Iddles, D. M.; Sinclair, D. C. *Appl. Phys. Lett.* **2003**, *82*, 4537.
(38) Tamura, H.; Konoike, T.; Sakabe, Y.; Wakino, K. *J. Am. Ceram. Soc.* **1984**, *67*, C59.

magnetic interactions between the Mn^{+IV} ions, which is presumably linked to the fact that 50% of the B-site cations are Ti^{+IV} and are therefore nonmagnetic. The partial ordering of the cations inferred from bond valence considerations can explain the unusual magnetism through the formation of strongly coupled spin trimers in a fraction of the three-site face-sharing octahedral units within the hexagonal regions of the structure. Impedance spectroscopy showed 12R-$BaTi_{1/2}Mn_{1/2}O_3$ to be a "leaky" dielectric; however, it exhibits high permittivity, $\epsilon_r \sim 45$, a modest quality factor, $Q \sim 2026$ (at 5.75 GHz), and a near-zero temperature coefficient of resonant frequency, $TC_f \sim -4$ ppm K^{-1}. The modest quality factor is attributed to the low dc resistivity of the material and to incomplete ordering of the cations on the B-sites and is likely to preclude any commercial applications of 12R-$BaTi_{1/2}Mn_{1/2}O_3$ as a microwave dielectric resonator, despite its high permittivity and near-zero TC_f.

Acknowledgment. We thank the EPSRC for funding (grant number GR/NO1095/01), for facilitating collaboration between Sheffield, Liverpool, and London Southbank Universities through the EPSRC-sponsored Perovskite Oxides and Microwave Dielectric Materials Networks, and for funding of neutron beam time at Rutherford Appleton Laboratories (RAL). We also thank Drs. Kevin Knight and Ron Smith at RAL for assistance in collecting the ND data.

CM035317N